J. Fluid Mech. (1983), *vol.* 127, *pp.* 123–140
Printed in Great Britain

An experimental study of the electrohydrodynamic flow in electrostatic precipitators

By G. L. LEONARD, M. MITCHNER AND S. A. SELF
High Temperature Gasdynamics Laboratory, Department of Mechanical Engineering, Stanford University, California 94305

(Received 3 December 1981)

Schlieren visualization and laser-anemometry experiments are presented which demonstrate that a two-dimensional positive corona discharge interacts with the flow of a wire–plate electrostatic precipitator to produce a non-turbulent secondary flow in a plane perpendicular to the discharge wires. Smoke-wire visualization and hot-wire anemometry experiments are then described which show that negative-corona-discharge non-uniformities are responsible for producing both secondary flow in a plane parallel to the discharge wire and also turbulence. The significance of these results to the performance of electrostatic precipitators is discussed.

1. Introduction

Electrostatic precipitators are extensively used to remove particulates from gases in a wide variety of industrial processes (White 1963). In the most common configuration, the gas flows horizontally with a velocity of 1–3 m/s through ducts formed by large vertical metal plates spaced typically 0·2–0·5 m apart. High-voltage wires are suspended in the midplane of each duct with a spacing approximately equal to the plate spacing. For applied voltages of the order of 50 kV, usually negative, a corona discharge is maintained between the wires and the grounded collector plates. Molecular ions are generated in the high electric field near the wires. The ions with the same polarity as the discharge wires migrate in the prevailing electric field through the gas to the plates, and constitute a discharge current. The particles entrained in the gas flow become electrically charged by the exposure to the ion flow, and then also migrate to the collector plates. The preciptated particulate layer is periodically rapped from the plates and falls into hoppers.

In modelling particle transport in precipitators it is generally assumed that the flow is sufficiently turbulent to distribute the particles uniformly in a direction perpendicular to the plates. This assumption is then used to transform the two-dimensional particle continuity equation into an ordinary first-order differential equation, which is then easily integrated to give the particle concentration as a function of the distance into the precipitator. From this concentration field the precipitator efficiency can be calculated. The resulting efficiency equation has come to be called the Deutsch formula.

In the present design of precipitators plate-stiffening baffles and large tubular discharge-wire supports are used, both of which produce high levels of wake turbulence. Therefore, the assumption of uniform particle distributions used in developing the Deutsch formula is likely valid for submicron-sized particles whose electric migration velocity is on the order of 5 cm/s or less. Recent theoretical and experimental work by the authors (Leonard, Mitchner & Self, 1980, 1982) has shown

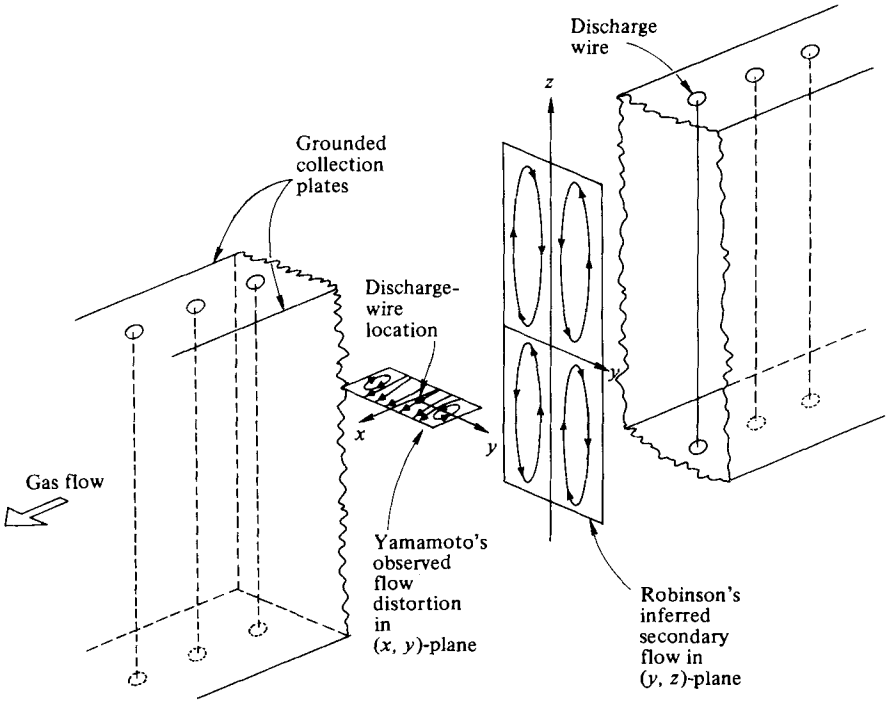

FIGURE 1. The secondary-flow patterns observed by Robinson and Yamamoto in wire–plate precipitators.

that for moderate levels of turbulence, e.g. fully developed turbulent channel flow, precipitators should be far more efficient than is predicted by the Deutsch formula. These results suggest that precipitators should be designed in a way to minimize the generation of turbulence.

The electrohydrodynamic (EHD) interaction of the corona discharge with the flow can also produce flow disturbances. The ions streaming through the gas exert a body-force on the gas, and depending on the current distribution can produce both secondary flow and turbulence. In fact, it has often been argued (Cooperman 1982) that corona-generated turbulence is sufficiently intense to justify the use of the Deutsch equation, and therefore any effort to reduce turbulence by designing precipitators in a streamlined manner would have no effect. The aim of the work presented here was to investigate the nature and magnitude of electrohydrodynamic generation of secondary flows and turbulence for typical wire–plate precipitator conditions.

Serious study of corona discharge (EHD) driven flows as applied to wire–plate precipitators began with the work of Robinson (1976), who used a helium tracer gas to map out convective and diffusive fluid transport in a precipitator similar to the one shown in figure 1. Robinson inferred that secondary flow in the form of vortical motion in the streamwise direction occurs when the precipitator is operated with positive-polarity corona discharge. (The discharge for positive corona is distributed continuously along the wire, whereas for negative corona the discharge tends to distribute itself in localized tufts along the wire.) It was also shown by Robinson that when the mean gas velocity is less than 3·0 m/s turbulence is produced at levels of corona-discharge current typically encountered in industrial precipitators (0·5 mA per metre of discharge wire).

Yabe, Mori & Hijikata (1978) performed experimental and analytical studies of secondary flow induced by positive corona discharge. The experimental apparatus consisted of a single discharge wire placed parallel to a grounded flat plate. These authors demonstrated that the effect of the corona discharge is to establish a distributed body force on the fluid. In the absence of cross-flow this body force induces two counter-rotating steady vortices located symmetrically on either side of the discharge wire in the region between the wire and the plate.

Yamamoto & Velkoff (1981) demonstrated both experimentally and analytically that a cross-flow acts to suppress the downstream vortex observed by Yabe *et al.* (1978). For discharge-current levels typical of precipitator applications the downstream vortex is completely eliminated when the mean gas velocity exceeds 0·5 m/s. The vortex previously upstream of the discharge wire moves downstream to a position opposite the discharge wire. The flow appeared to be steady in time, with the streamlines taking the form shown in figure 1. The region of vortical (recirculating) flow opposite the discharge wires increases in size as the current is increased and as the mean gas velocity is decreased. These results appeared to be inconsistent with both the secondary flow pattern ((y, z)-plane) and increase in turbulence level observed by Robinson.

Experimental results are presented in this paper which resolve the differences between Yamamoto's and Robinson's findings and give a more complete picture of the effect of positive corona discharge on precipitator flows. Schlieren visualization and laser-anemometry results are presented which are in accord with the two-dimensional study of Yamamoto for the positive-polarity case. These results should be useful in making a quantitative comparison with numerical calculations. Hot-wire anemometry and smoke-wire visualization results for the positive-corona-discharge case are presented which demonstrate the origins of the secondary and turbulent flows observed by Robinson.

Hot-wire and smoke-wire studies performed for the negative corona case are also presented. These studies show that the negative corona discharge, unlike the positive corona discharge, produces turbulence throughout the precipitator.

2. Single-wire and plate precipitator experiments

In this section we present the results of experiments that were designed to study the gas flow field in the single-wire precipitator (wire–plate precipitator with one wire energized) shown in figure 2. We begin by presenting schlieren photographs of the gas flow field subjected to positive corona discharge. Laser-anemometry (LDV) results are then presented which confirm the schlieren results and add quantitative detail to the description of the flow field. Hot-wire measurements taken downstream of the single-wire precipitator operating with positive corona discharge are then presented. These studies show that except for large values of the dimensionless number $i/lb\rho u_0^2$, which is a measure of the ratio of the corona-discharge- (or EHD) induced body force to the inertial force on the gas,† the flow is non-turbulent in the centre of the channel (i.e. away from the endwalls through which the corona discharge wire passes). Here i/l is the discharge current per unit length of discharge wire, b is the ion mobility, ρ is the gas density and u_0 is the mean gas velocity at the inlet to the precipitator.

† The body force per unit volume on the gas is given by J/b, where J is the magnitude of the current density vector and b is the ion mobiity. When the term J/b is divided by the inertial force per unit volume $\rho u_0^2/d$, where d is the wire-to-plate spacing and J is normalized by i/ld, the ratio $i/\rho lbu_0^2$ is obtained.

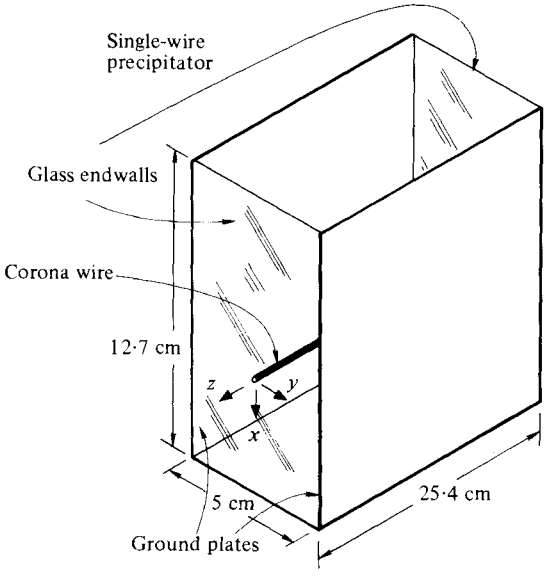

FIGURE 2. Single-wire precipitator geometry.

The hot-wire results show that turbulence is produced near the endwalls, with the regions of turbulence growing towards the channel centre for increasing values of $i/lb\rho u_0^2$. Smoke-wire visualization results are presented which demonstrate the origins of the positive corona-discharge-induced endwall turbulence, and how Robinson's and Yamamoto's findings can be reconciled. Finally, smoke-wire visualization results are presented for the negative corona discharge. In contrast with the uniform and symmetric discharge structure of a positive corona, the discharge from a negative corona is highly non-uniform and unsteady, with current originating from discrete points on the wire. These results demonstrate the importance of the corona-discharge structure on the precipitator flow and that corona-induced turbulent mixing is significantly reduced by increasing the precipitator's mean gas velocity (and therefore decreasing the number $i/lb\rho u_0^2$).

2.1. *Schlieren visualization results*

Shown in figure 3 is a schematic diagram of the schlieren visualization apparatus. Two thin stainless-steel electrically heated wires (0·2 mm diameter) were placed upstream (6·35 cm) of the corona discharge wire of diameter 0·2 mm. One upstream wire was placed 0·5 cm from the ground plane and the other was placed at the tunnel midplane. The plate-to-plate spacing of the single-wire precipitator was 5·0 cm. As the flow passed near the wires it became heated. The thermal wakes of the wires were observed with the schlieren optical system and recorded on Polaroid type 57 film using a Sinar camera. The measured free-stream turbulence level upstream of the precipitator was less than 0·2 % and the mean gas velocity was uniform across the core of the flow to within $\pm 0{\cdot}3\,\%$.

Shown in figure 4 are schlieren photographs for the case where the upstream mean gas velocity u_0 (cross-flow velocity) was 1·0 m/s. The linear current density was 0, 1·0, 2·0 and 3·0 mA/m (positive polarity) for figures 4(*a*), (*b*), (*c*) and (*d*) respectively. These conditions correspond to values of the dimensionless number $i/lb\rho u_0^2$ of 0, 5·2, 10·4 and 15·6 respectively. The gas flows from top to bottom in these figures, with

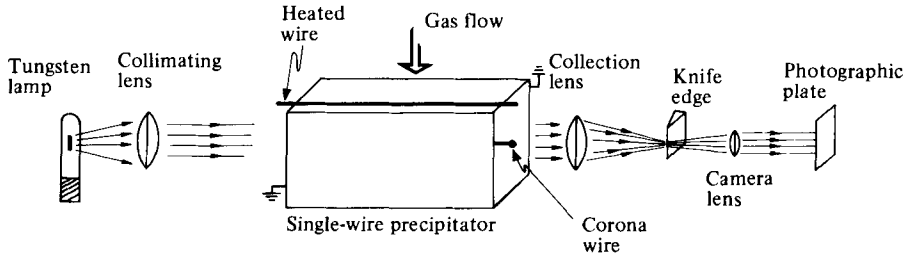

FIGURE 3. Schlieren visualization system.

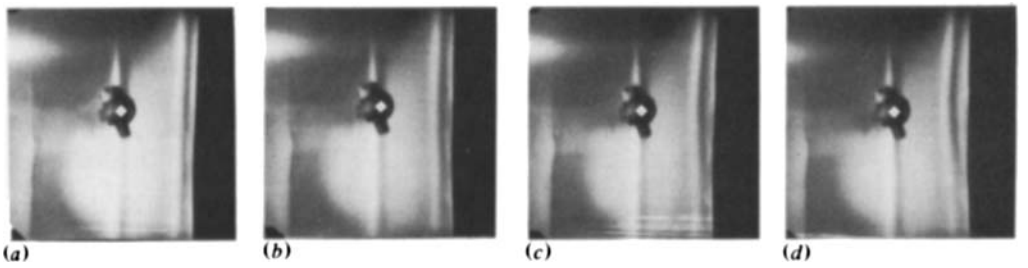

FIGURE 4. Schlieren visualization results; mean gas velocity $u_0 = 1{\cdot}0$ m/s: (*a*) $i/l = 0$ mA/m; (*b*) 1·0 mA/m; (*c*) 2·0 mA/m; (*d*) 3·0 mA/m.

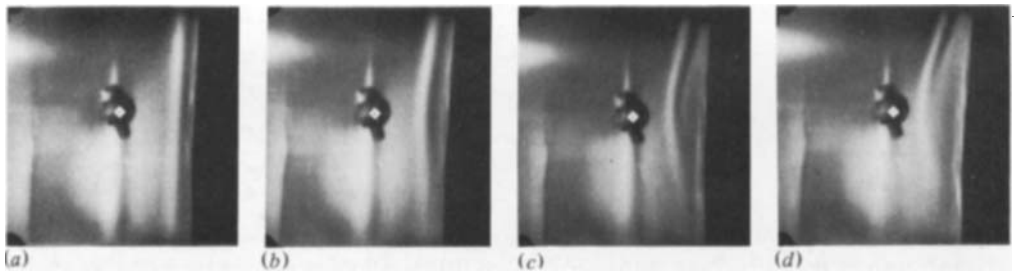

FIGURE 5. Schlieren visualization results; mean gas velocity $u_0 = 2{\cdot}0$ m/s: (*a*) $i/l = 0$ mA/m; (*b*) 1·0 mA/m; (*c*) 2·0 mA/m; (*d*) 3·0 mA/m.

the right ground plane appearing black and the left one appearing greyish-white. The white diamond denotes the approximate location of the discharge wire. These flow fields are in agreement with those observed by Yamamoto. The upstream streamline nearest the ground wall bends towards the discharge wire. Downstream of the discharge wire this streamline curves back towards the ground wall, indicating that a recirculating region of flow has been established opposite the discharge wire and near the ground wall. In figure 5 the mean-flow velocity u_0 was changed to 2·0 m/s. The value of the dimensionless number $i/lb\rho u_0^2$ is 0, 1·3, 2·6 and 3·9 for figures 5(*a*), (*b*), (*c*) and (*d*) respectively. The regions of recirculating flow were reduced in size as predicted by Yamamoto. For a typical industrial precipitator the dimensionless number $i/lb\rho u_0^2$ would range from 0·2 to 2·0. From figures 4 and 5 we observe that flow distortion in the (x, y)-plane as observed by Yamamoto only becomes significant at values of the dimensionless number $i/lb\rho u_0^2$ higher than is generally encountered in practical precipitators.

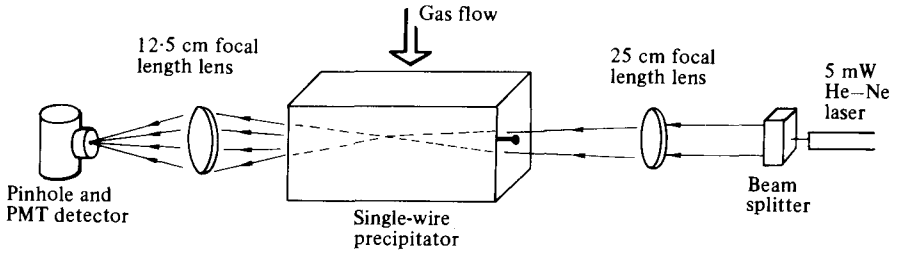

FIGURE 6. Laser-anemometry system.

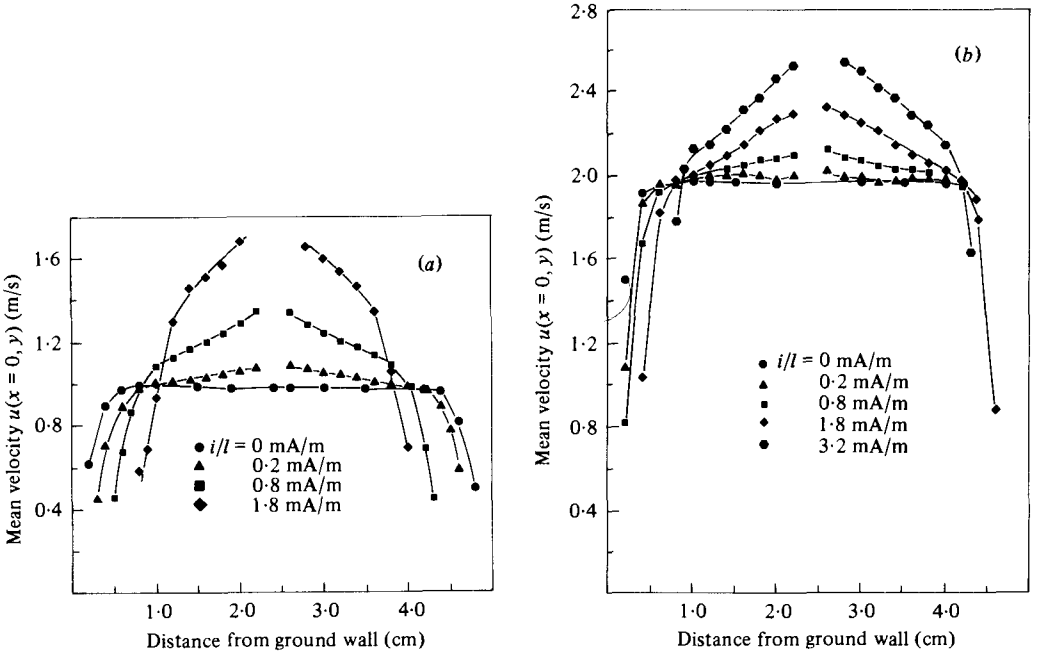

FIGURE 7. Laser-anemometry results for (*a*) $u_0 = 100$ cm/s and (*b*) $u_0 = 200$ cm/s.

2.2. *Laser-anemometry results*

In using the laser anemometer in a precipitator to make gas-velocity measurements one has to be certain that the velocity of the seed particles is the same as the gas velocity. For any particular component of gas velocity of interest, this condition will be satisfied provided that the component of the Coulomb force acting on the particles in this direction is zero. For the single-wire precipitator shown in figure 3 with positive corona discharge, there exists a transverse symmetry plane passing through the wire ($x = 0$) in which the electric field vector must lie. Therefore, the axial component of gas velocity $u(x = 0, y)$ can be measured in this plane. These measurements were made with a laser anemometer operating in forward scatter as shown in figure 6. The signal was detected with a TSI Model 9162 photomultiplier and processed with a TSI Model 1096 frequency counter. The flow was seeded with oleic-acid droplets, which were generated with a spinning-disk aerosol generator and had a diameter of 4·0 μm.

In figure 7(*a*) the gas velocity profile $u(x = 0, y)$ is plotted versus transverse distance y for several different values of the linear current density (positive corona).

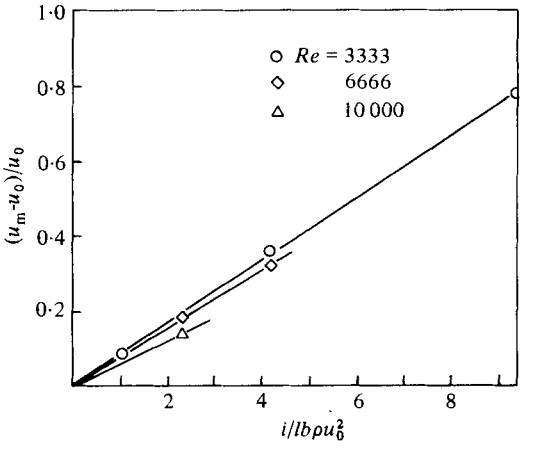

FIGURE 8. Fractional increase in centreline gas velocity versus the dimensionless parameter $i/lb\rho u_0^2$.

The gas velocity $u(x = 0, y)$ for the case of zero current density is also shown and corresponds to a mean gas velocity of 1·0 m/s. Note that, as the linear current density is increased, the centreline velocity increases. At a linear current density of 1·8 mA/m ($i/lb\rho u_0^2 = 9{\cdot}4$) the mean velocity near the channel centre ($y = 2{\cdot}5$ cm) is 60–80 % greater than the velocity at zero current density. Velocity measurements could not be made near the discharge wire since all the seed particles had migrated out of this region. At the highest current density the velocity profile is decreasing rapidly in a region far from the wall (approx. 1·0 cm), indicating that a recirculating region of flow exists near the wall as predicted by Yamamoto and observed with the schlieren photographs. The velocity field was completely steady in time (non-turbulent) at the measurement locations.

Shown in figure 7 (*b*) are similar studies with the mean velocity at zero current density increased to 2·0 m/s. Again there was no measurable level of turbulence induced by the corona discharge. As the linear current density is increased, the core velocity increases at the expense of the wall velocity as in the case of figure 7 (*a*). Note that for a given linear current density the percentage increase in velocity is lower in figure 7 (*b*) than in figure 7 (*a*), in accord with the schlieren photographs.

Plotted in figure 8 is the percentage increase in mean gas velocity at $y = 2{\cdot}5$ cm (obtained by extrapolation with straight lines through the data) as a function of the dimensionless number $i/lb\rho u_0^2$. For a given Reynolds number (based upon mean velocity at zero current) the percentage increase in velocity is proportional to the dimensionless number $i/lb\rho u_0^2$. From figure 8 we see that the Reynolds-number dependence is small, in comparison with the dependence on $i/lb\rho u_0^2$. This comparison suggests that the dimensionless number $i/lb\rho u_0^2$ is the dominant parameter in establishing similarity in the flow field for the positive corona discharge case. For a full-scale industrial precipitator we see from figure 8 that we would expect less than a 10 % increase in the centreline velocity.

2.3. *Hot-wire anemometry results*

In order to detect the generation of turbulence in the single-wire precipitator for the positive corona discharge case, a TSI Model 1050 hot-wire anemometer was used to make turbulence-intensity measurements downstream of the single-wire precipitator.

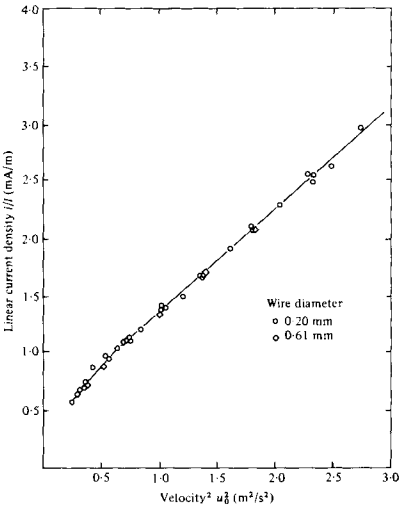

FIGURE 9. Current levels at which centreline instability occurred.

Initially, the anemometer was traversed in the y-direction (ground plane to ground plane) midway between the endwalls and 11·5 cm downstream of the discharge wire. It was found that for moderate values of linear current density there was no generation of turbulence. When the hot wire was traversed in the z-direction (along the direction of the discharge wire) midway between the ground planes it was found that turbulence was being generated near the endwalls. As the linear current density was increased, the boundaries of the turbulent-flow regions migrated inwards from the endwalls towards the centre (x, y)-plane of the channel. Show in figure 9 are the linear current densities at which turbulence was first detected for increasing current at the tunnel centreline (11·5 cm downstream of the discharge wire and 12·5 cm from each endwall), plotted against the mean velocity squared u_0^2 (as measured upstream of the single wire precipitator). The linearity of the data again suggests that the dimensionless ratio $i/lb\rho u_0^2$ is the dominant number in establishing similarity.

2.4. *Smoke-wire visualization results*

A smoke-wire visualization technique was used to study the endwall-generated turbulence noted in §2.3. The experimental arrangement is shown in figure 10. Five tantalum wires, each 0·18 mm in diameter, were placed perpendicular to the flow 6·35 cm downstream of the discharge wire. Each wire was coated with mineral oil and then resistively heated with 60 Hz a.c. The mineral oil evaporated and then quickly recondensed, forming sheets of smoke whose motion downstream of the precipitator was recorded photographically.

Shown in figures 11 (*a–e*) are the results obtained for a mean gas velocity of 1·25 m/s. Figure 11 (*a*) corresponds to the case of zero current. The three sheets of smoke in the centre look like fine filaments when viewed from the side. Near the endwalls the smoke sheets have bowed somewhat as a result of a slight secondary corner flow generated in the upstream nozzle.

Figure 11 (*b*) shows the flow pattern for a linear current density of 0·2 mA/m (positive polarity, $i/lb\rho u_0^2 = 0{\cdot}67$). Although the flow in the channel centre is undisturbed, the flow near the endwalls is significantly altered. When viewed as a function of time this induced corner flow is steady (non-turbulent) and takes the form of vortices whose axes are aligned with the x-direction.

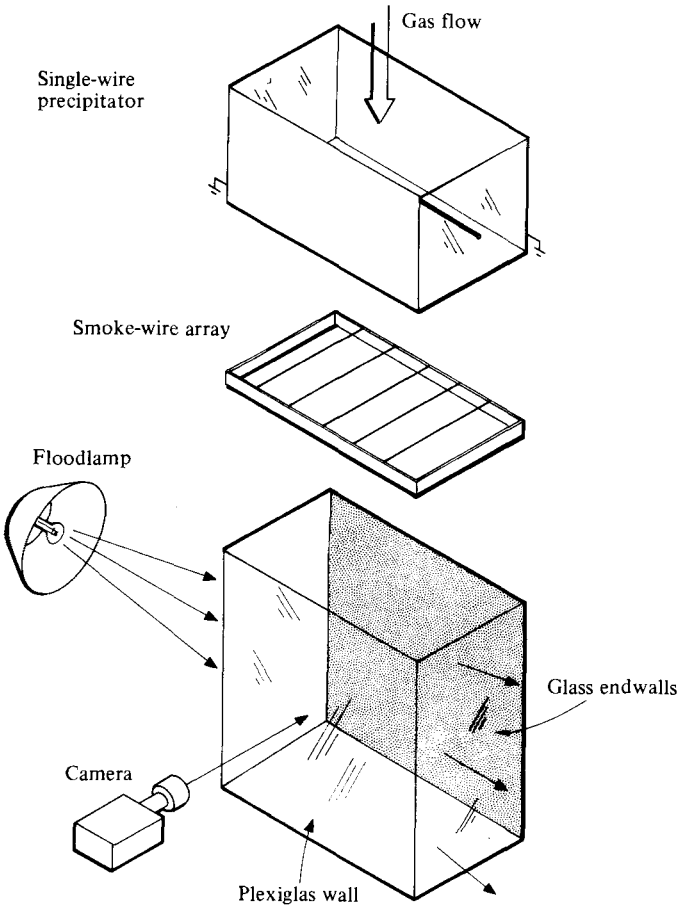

FIGURE 10. Smoke-wire visualization system.

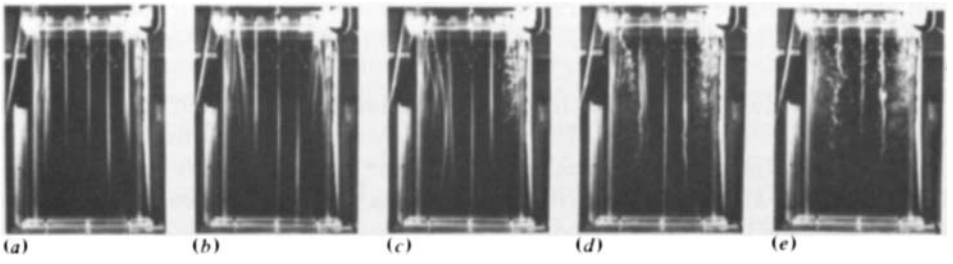

FIGURE 11. *Smoke-wire visualization results; single-wire precipitator; positive corona; mean gas* velocity $u_0 = 1{\cdot}25$ m/s: (*a*) $i/l = 0$ mA/m; (*b*) 0·2 mA/m; (*c*) 0·4 mA/m; (*d*) 1·0 mA/m; (*e*) 2·0 mA/m.

In figure 11 (*c*) the linear current density is 0·4 mA/m ($i/lb\rho u_0^2 = 1{\cdot}34$). The induced vortical motion has become turbulent at one endwall. For increasing linear current densities the regions of turbulent flow move toward the centre of the tunnel. This behaviour is consistent with the hot-wire results of §2.3 and would account for the increased turbulence level Robinson observed.

In figures 12(*a–e*) similar smoke-wire photographs are shown for a mean gas

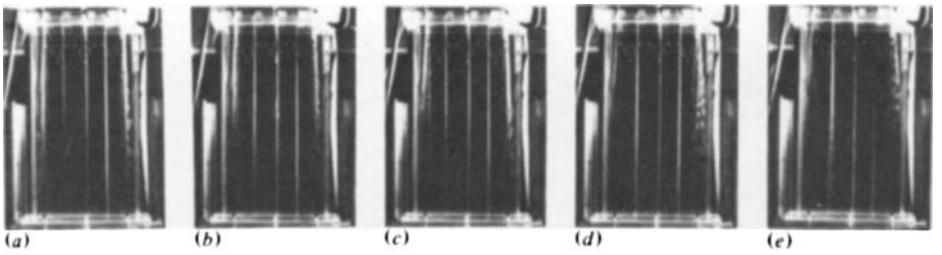

FIGURE 12. Smoke-wire visualization results; single-wire precipitator; positive corona; mean gas velocity $u_0 = 3{\cdot}31$ m/s: (*a*) $i/l = 0$ mA/m; (*b*) 0·2 mA/m; (*c*) 0·4 mA/m; (*d*) 1·0 mA/m; (*e*) 2·0 mA/m.

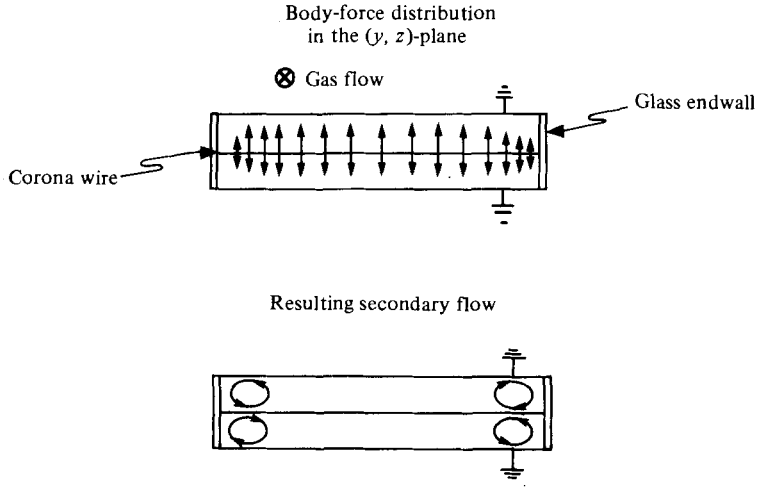

FIGURE 13. A schematic representation of the body-force distribution resulting from the corona quenching at the endwalls and the secondary flow this distribution drives.

velocity of 3·31 m/s. At the higher velocity the region of corona-induced secondary motion and turbulence production is confined to the vicinity of the endwalls. Again it should be noted that all the results presented to this point are for the positive corona discharge.

The secondary flow induced by the corona discharge, as observed in figures 11 and 12, appears to occur as a result of corona quenching by the insulating endwalls of our precipitator. Visual observations show that the corona current is quenched near the Plexiglas endwalls, as would be expected from a build-up of static charge on these walls. The resulting body-force distribution on the gas is shown schematically in figure 13. This body-force distribution appears to drive the secondary flow shown in figures 11 and 12.

These measurements appear to resolve the apparent contradiction between Yamamoto's and Robinson's observations. Yamamoto predicted and viewed motion in the (x, y)-plane. He did not see motion in the (y, z)-plane near his discharge-wire termination because the electrically heated wires in his schlieren system were about one-half the length of the corona wire, thereby reducing the possibility of detecting flow effects produced by the corona-wire termination. (In addition, the schlieren technique is a line-of-sight method capable of detecting flow distortion only in the perpendicular plane.) Robinson's wind tunnel had a small aspect ratio (3:1), and

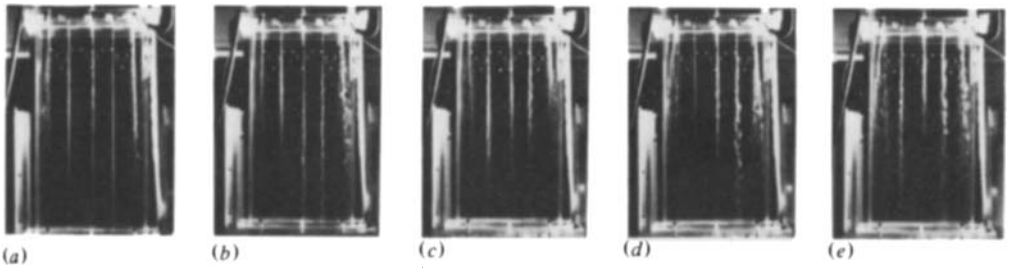

FIGURE 14. Smoke-wire visualization results; single-wire precipitator; negative corona; mean gas velocity $u_0 = 1{\cdot}25$ m/s: (*a*) $i/l = 0$ mA/m; (*b*) 0·2 mA/m; (*c*) 0·4 mA/m; (*d*) 1·0 mA/m; (*e*) $i/l = 2{\cdot}0$ mA/m.

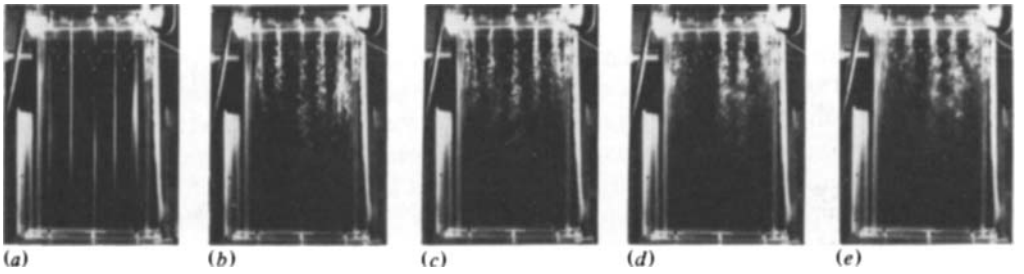

FIGURE 15. Smoke-wire visualization results; single-wire precipitator; negative corona; mean gas velocity $u_0 = 3{\cdot}31$ m/s; (*a*) $i/l = 0$ mA/m; (*b*) 0·2 mA/m; (*c*) 0·4 mA/m; (*d*) 1·0 mA/m; (*e*) 2·0 mA/m.

therefore the flow he investigated was likely dominated by the endwall effects shown in figures 11 and 12. (In full-scale precipitators the aspect ratios are much larger (30–60:1) and the endwall effects would not be expected to be a dominant factor influencing precipitator performance. The endwall geometry is also quite different from the simple configurations used in this work, and in the experiments of Yamamoto and Robinson.)

As noted in §1, most industrial precipitators use negative corona discharge. Smoke-wire visualization experiments were also performed for this case. The results are shown in figures 14 and 15, where the mean flow velocities are 1·25 and 3·31 m/s respectively. In contrast with the positive-corona case, the velocities in the core of the channel flow field are observed to be turbulent (thereby leading to increased mixing) for all values of current and velocity. The mixing is appreciably reduced with increasing values of mean gas velocity u_0. In addition, there is evidence of vortical flow generated near the endwalls, similar to that observed for the positive-corona-discharge case. Again this flow is due to the quenching of the negative corona at the endwalls.

The core-turbulence generation by the negative corona appears to result from the three-dimensional tuft-like structure of the negative corona. The localized corona tufts probably act to induce local secondary flows, which are unstable and lead to turbulence production.

3. Multiwire and plate precipitator experiments

Experiments with seven discharge wires were performed to determine the degree to which the information obtained with the single-wire precipitator is applicable to

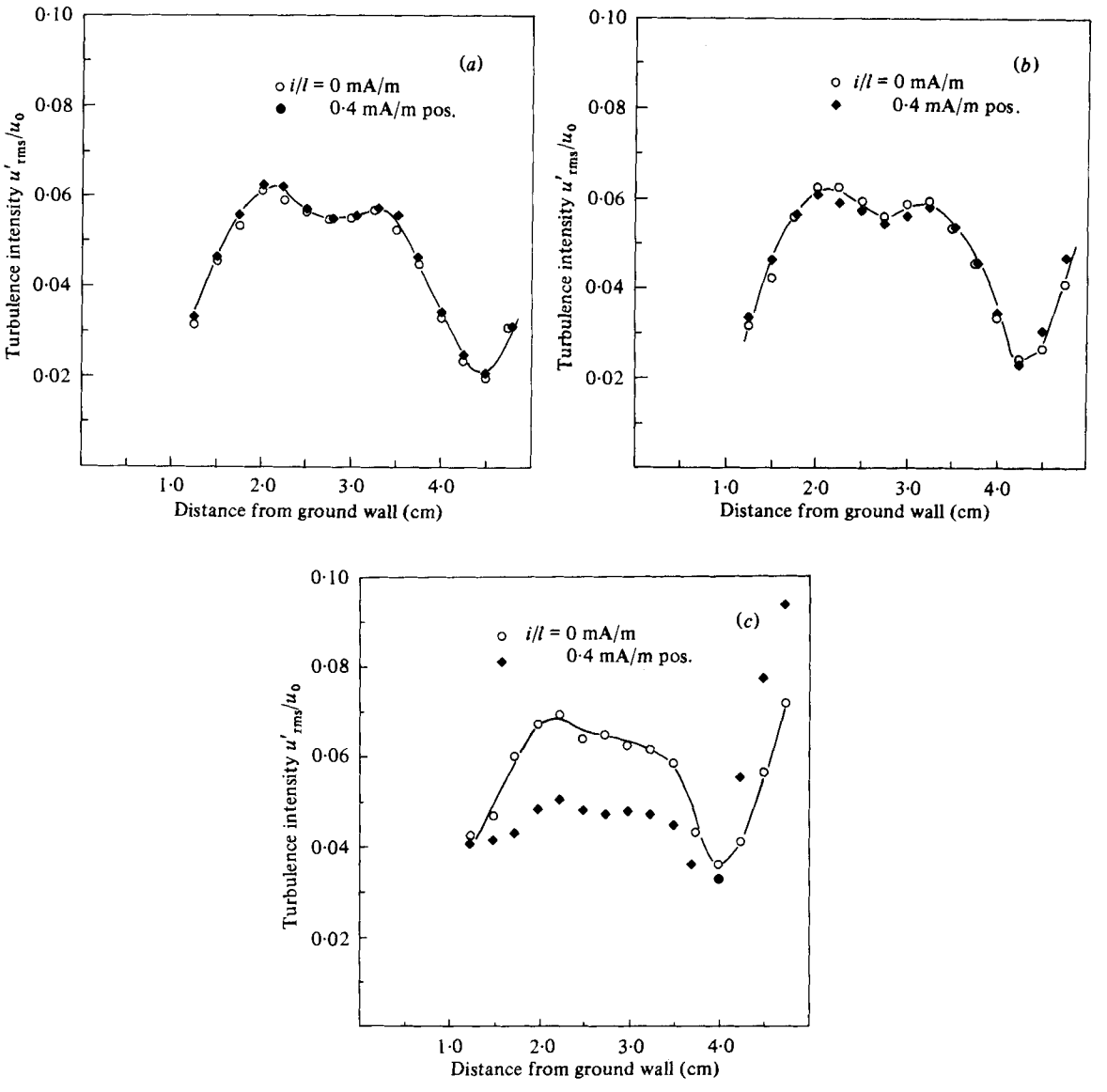

FIGURE 16. Turbulence-intensity measurements for (*a*) $u_0 = 331$ cm/s; (*b*) $u_0 = 220$ cm/s; (*c*) $u_0 = 125$ cm/s. Multiwire precipitator; positive-corona discharge.

a multiwire precipitator. The hot-wire anemometer was used to make turbulence-intensity measurements downstream of the precipitator. Flow patterns downstream of the multiwire precipitator were studied with the smoke-wire visualization technique described previously.

The multiwire precipitator has a plate-to-plate spacing of 5·0 cm, a wire-to-wire spacing of 5·08 cm and a wire radius of 0·44 mm. This value of the corona wire radius was chosen so as to obtain geometric similarity between this precipitator and an industrial precipitator.

3.1. *Hot-wire anemometry results*

The hot-wire probe was traversed in the transverse (or y-direction) midway between the ground plates and 17·8 cm downstream of the seventh and last discharge wire. The first series of experiments were performed with positive corona discharge. Shown in figure 16(*a*) are turbulence-intensity measurments made for the case of a mean gas velocity of 3·31 m/s. Plotted are measurements with the linear current density equal to 0 and 0·4 mA/m ($i/lb\rho u_0^2 = 0$ and 0·19 respectively). As expected, there was no increase in turbulence level beyond that produced by the wakes of the unenergized discharge wires. Figure 16(*b*) shows similar results for a mean gas velocity $u_0 = 2{\cdot}20$ m/s.

As shown in figure 16(*c*), the turbulence intensity at a mean gas velocity of 1·25 m/s ($i/lb\rho u_0^2 = 1{\cdot}6$) is observed, somewhat surprisingly, to decrease when the corona discharge is energized. A possible explanation of this behaviour is that the kinematic viscosity of the air is increased locally by the corona current. With the discharge absent the Reynolds number of the flow around the wire, based on wire diameter, is large enough to establish a turbulent wake. When the discharge is activated the current density near the wire is high enough to heat the flow locally (as observed during the schlieren experiments), thus raising the kinematic viscosity of the air. The Reynolds number of the flow about the wires is therefore decreased to a level at which the wake becomes quasistable, thereby leading to a slightly reduced core turbulence intensity level. It is possible also (for reasons that are not readily apparent) that the corona-induced body force alters the turbulent structure of the wire wakes in a manner so as to reduce the turbulence intensity.

The more interesting feature of the flow field shown in figure 16(*c*) is the increase in turbulence intensity observed near the ground wall ($y = 5{\cdot}0$ cm). This increase results from the spreading inwards of the secondary and turbulent flow generated at the endwalls.

The results of similar experiments performed with negative corona discharge are presented in figures 17(*a–c*). For the data in figure 17(*a*) the mean gas velocity u_0 was 3·31 m/s and the linear current density was 0 and 0·4 mA/m ($i/lb\rho u_0^2 = 0$ and 0·19 respectively). The corona discharge appears simply to smooth the turbulence profile with little, if any, increase in the total turbulent energy. A similar conclusion can be drawn from figure 17(*b*), where the mean gas velocity $u_0 = 2{\cdot}20$ m/s ($i/lb\rho u_0^2 = 0{\cdot}43$). Figure 17(*c*) shows the case for a mean velocity $u_0 = 1{\cdot}25$ m/s ($i/lb\rho u_0^2 = 1{\cdot}33$). Here we see a marked increase in the turbulence intensity above the level established by the wakes of the unenergized discharge wires.

Shown in figure 18 are turbulence-intensity measurements for the negative-corona-discharge case made at the tunnel centre ($y = 2{\cdot}5$ cm) plotted against mean gas velocity u_0. A sharp increase in turbulence intensity is observed when the gas velocity is decreased below 2·0 m/s. The scatter shown in the data occurs because of the well-known unsteady nature of negative coronae. The discharge tufts were observed to change position in time, making downstream measurements non-reproducible. For the values of linear current density and mean gas velocities tested, endwall-generated turbulence should not have made a contribution to u'_{rms}/u_0 in figure 18.

The data presented in figure 18 suggests that the core turbulence generated by the negative corona discharge is only noticeable for values of the dimensionless number $i/lb\rho u_0^2$ greater than 0·5. For values less than 0·5 the turbulence generated by the wake of the discharge wires, which is significantly less than the turbulence generated by

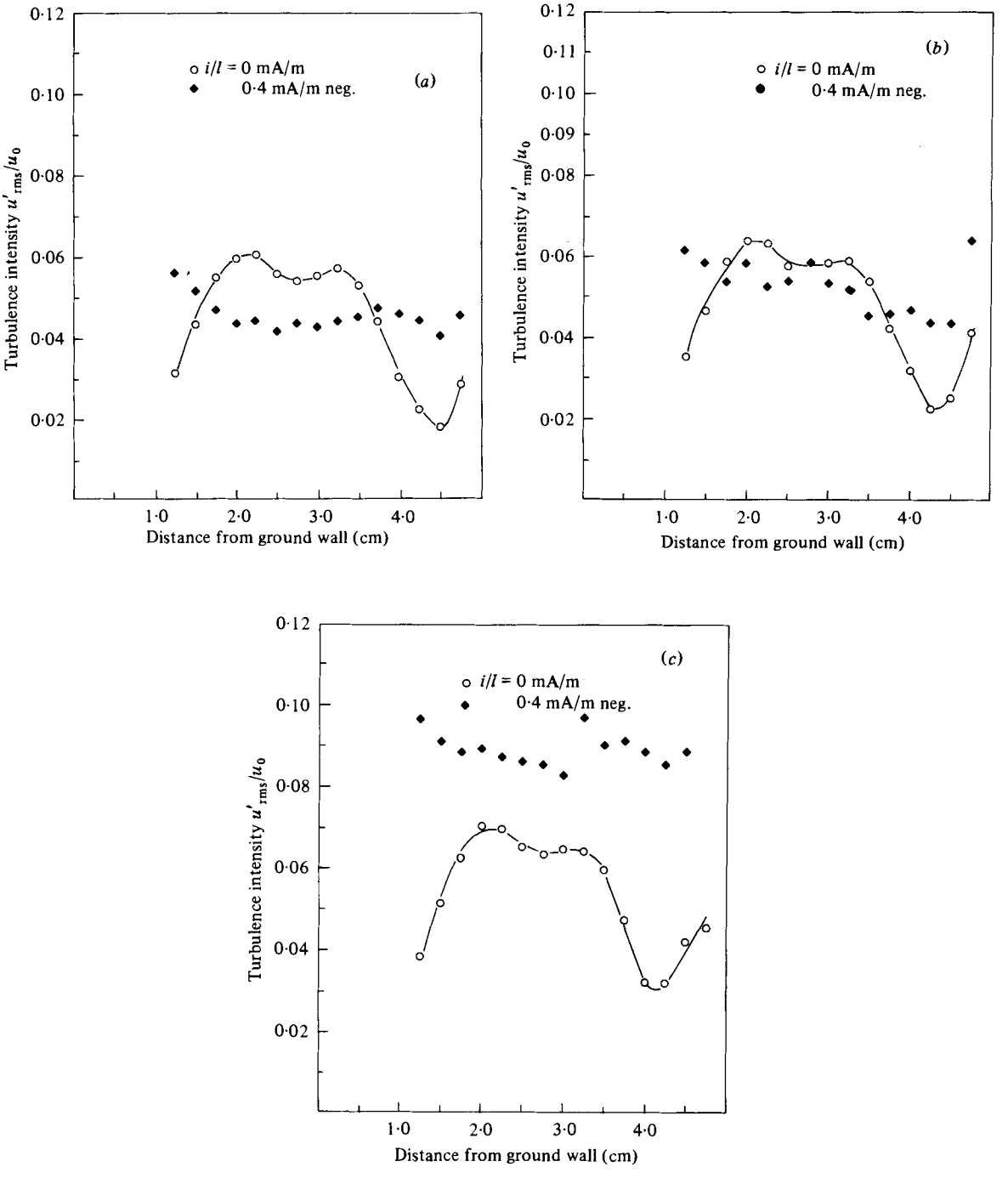

FIGURE 17. Turbulence intensity measurements for (*a*) $u_0 = 331$ cm/s; (*b*) $u_0 = 220$ cm/s; (*c*) $u_0 = 125$ cm/s. Multiwire precipitator; negative-corona discharge.

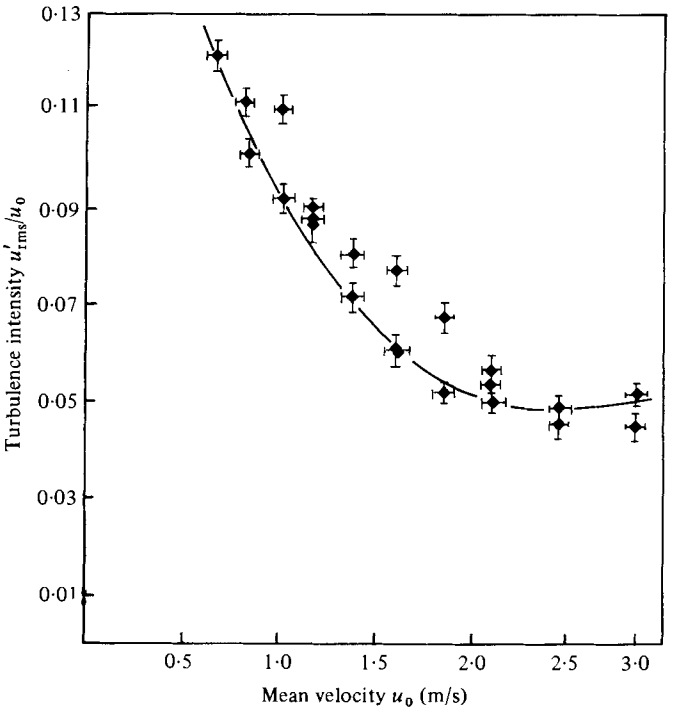

FIGURE 18. Centreline turbulence intensity versus mean gas velocity for a linear current density of 0·4 mA/m. Multiwire precipitator; negative corona.

the plate-stiffening baffles and discharge-wire supports used in industrial precipitators, masks any corona-discharge-induced turbulence.

3.2. *Smoke-wire visualization results*

The smoke-wire technique was used to study the flow downstream of the multiwire precipitator. Again five wires were coated with mineral oil and heated, thereby forming sheets of smoke whose motion was then photographed.

Shown in figures 19 (*a–f*) are results for a mean gas velocity of 1·25 m/s. Figures 19 (*a–c*) are for positive coronae, figures 19 (*d–f*) are for negative coronae. In figure 19 (*a*) the linear current density is zero. In this case the smoke shows the dispersion associated with the turbulent wakes of the unenergized discharge wires. When the linear current density was set equal to 0·2 mA/m (figure 19 (*b*), $i/lb\rho u_0^2 = 0{\cdot}67$) the turbulence associated with the vortical corner flow was again observed near the endwall, as in the single-wire precipitator configuration with positive corona discharge discussed earlier. In the seven-wire case the motion extends further from the endwalls and is more pronounced than in the single-wire case. Each wire makes a contribution to the motion, as would be expected.

For the negative-corona case we again see evidence of the turbulence associated with the endwall vortical motion. We also see increased turbulence throughout the precipitator, in contrast with the behaviour with positive-corona discharge. The results of a similar experiment for a mean gas velocity of 3·31 m/s are presented in figures 20 (*a–f*). The endwall turbulent motion tends to be suppressed at the higher velocity, as was the case for the single-wire precipitator. At the higher velocity, any

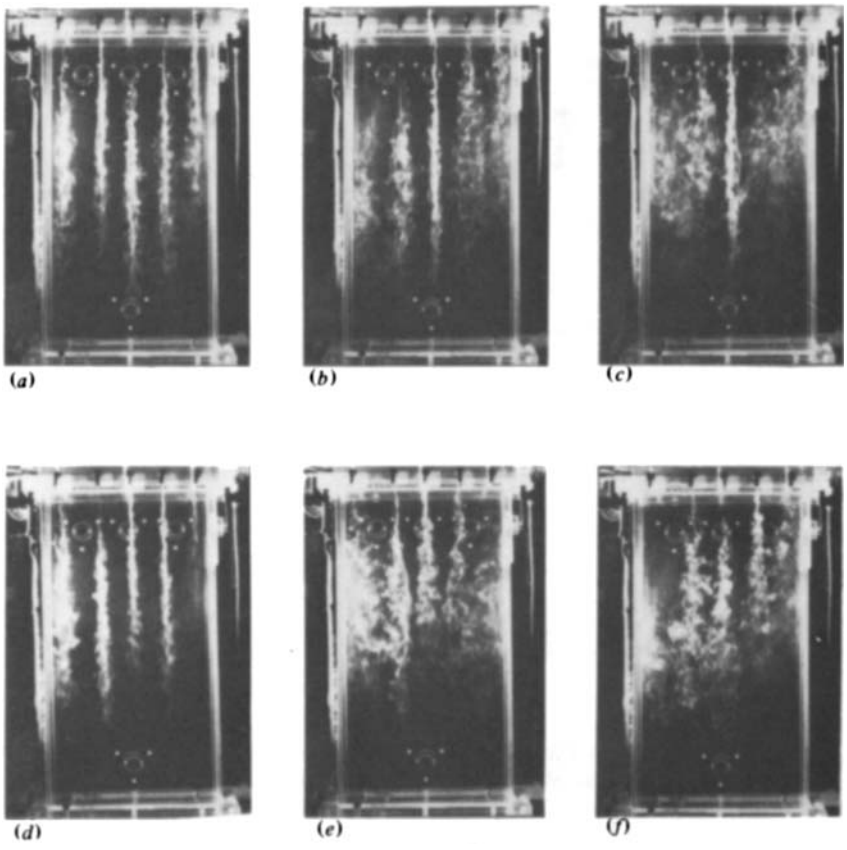

FIGURE 19. Smoke-wire visualization results; multiwire precipitator; (*a*)–(*c*) positive corona; (*d*)–(*f*) negative corona; $u_0 = 1{\cdot}25$ m/s: (*a*), (*d*) $i/l = 0$ mA/m; (*b*), (*e*) 0·2 mA/m; (*c*), (*f*) 0·4 mA/m.

mixing induced by the corona discharge in both the positive- and negative-corona-discharge cases is masked by the wake turbulence of the discharge wires, which is present even in the absence of the corona discharge.

4. Conclusions

To obtain an understanding of how secondary and turbulent flows are generated by a corona discharge in a wire–plate precipitator several experiments were performed. Schlieren and laser-anemometry results were obtained which support the findings of Yamamoto & Velkoff (1981) for the positive-corona-discharge case. In the plane perpendicular to the corona wire, the flow separates from each wall upstream of the corona-discharge wire and reattaches downstream leaving regions of recirculating flow opposite the wires near each wall. The velocity in the core of the flow is increased. For conditions typical of a large-scale precipitator the centreline velocity would be expected to increase by less than 10%. The fluid motion, as studied using both schlieren and laser anemometry methods, lies entirely in the (x, y)-plane of figure 2. The fluid motion was observed to be non-turbulent in the core of the flow.

Hot-wire anemometry measurements downstream of a single-wire precipitator demonstrate that turbulence is generated in the positive-corona case near the endwalls of the channel. This feature of the flow was confirmed with a smoke-wire

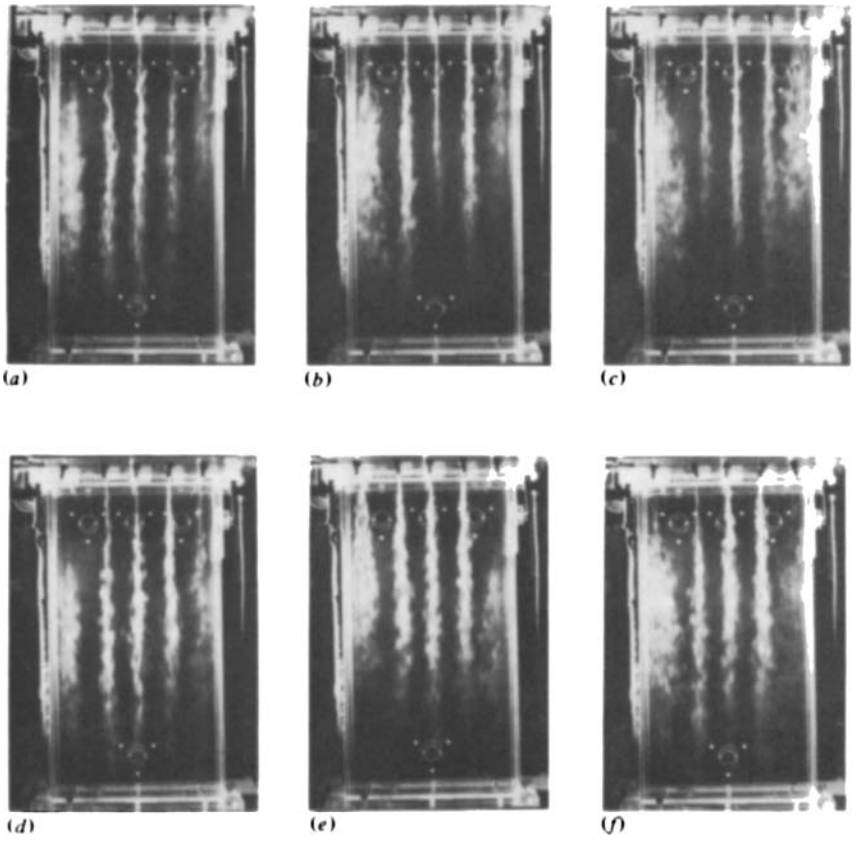

FIGURE 20. Smoke-wire visualization results; multiwire precipitator; (*a*)–(*c*) positive corona; (*d*)–(*f*) negative corona; $u_0 = 3{\cdot}31$ m/s: (*a*), (*d*) $i/l = 0$ mA/m; (*b*), (*e*) 0·2 mA/m; (*c*), (*f*) 0·4 mA/m.

visualization technique. The smoke-wire technique shows the generation of streamwise vorticity in the corners near the precipitator endwalls. This motion becomes turbulent as the linear current density is increased. It appears that this corner flow is driven by a non-uniform body force that results from the quenching of the corona discharge at the tunnel endwalls. The motion observed is consistent with that seen by Robinson when the endwall effects extend to the tunnel centreline. For precipitators with a large aspect ratio the positive-corona discharge would appear not to produce any core turbulence.

Hot-wire measurements conducted in a multiwire precipitator (seven energized wires) demonstrate that for positive corona no turbulence is produced aside from endwall effects. Smoke-wire visualization showed that again vortical motion in the (y, z)-plane is induced near the tunnel endwalls. With negative-corona discharge, the level of turbulence intensity in the core of the flow was observed to increase in excess of the background turbulence level when the mean gas velocity was less than 2·0 m/s ($i/lb\rho u_0^2 > 0{\cdot}5$). This augmented level of turbulence is likely produced by unstable secondary flows generated near the discharge tufts of the negative-corona discharge. For mean gas velocities larger than 2·0 m/s ($i/lb\rho u_0^2 < 0{\cdot}5$) no change in turbulence intensity was observed when the negative-corona discharge was energized.

The implications of these results with respect to the design of more-efficient (or

smaller) precipitators may be summarized as follows. For typical dimensions, mean gas velocities, and current densities, the interaction between the gas flow and the corona discharge should be relatively weak for $i/lb\rho u_0^2 < 0{\cdot}5$. For positive-corona discharge the interaction will result in the formation of a steady secondary flow pattern, while for negative polarity the turbulence will be increased when $i/lb\rho u_0^2 > 0{\cdot}5$. For typical electrostatic-precipitator conditions, the level of corona-induced turbulence is significantly smaller than that resulting from entrance ducting and the wakes of internal structures typical of commercial precipitators. It therefore appears that corona-induced turbulence does not represent an inherent obstacle to the achievement of improved precipitator performance through improved turbulence control.

This work was supported by the National Science Foundation under Grant no. CPE-7926290 and in part by the Electric Power Research Institute under Contract RP-533-1.

REFERENCES

COOPERMAN, P. 1982 Particle transport in electrostatic precipitators. Discussions. *Atmos. Environ.* **16**, 1568–1571.

LEONARD, G. L., MITCHNER, M. & SELF, S. A. 1980 Particle transport in electrostatic precipitators. *Atmos. Environ.* **14**, 1289–1299.

LEONARD, G. L., MITCHNER, M. & SELF, S. A. 1982 An experimental study of the effect of turbulent diffusion on precipitator efficiency. *Aerosol Sci.* **13**, 271–284.

ROBINSON, M. 1976 Effects of the corona discharge on electric wind convection and eddy diffusion in an electrostatic precipitator. Ph.D. thesis, The Cooper Union University.

WHITE, H. J. 1963 *Industrial Electrostatic Precipitators.* Addison-Wesley.

YABE, A., MORI, Y. & HIJIKATA, K. 1978 EHD study of the corona wind between wire and plate electrodes. *A.I.A.A. J.* **16**, 340–345.

YAMAMOTO, T. & VELKOFF, H. R. 1981 Electrohydrodynamics in an electrostatic precipitator. *J. Fluid Mech.* **108**, 1–18.